Vol. 36, No. 10, October 1998

Unsteady Stall Control Using Dynamically Deforming Airfoils

M. S. Chandrasekhara*
U.S. Naval Postgraduate School, Monterey, California 93943
M. C. Wilder†
MCAT, Inc., Mountain View, California 94043
and
L. W. Carr‡
NASA Ames Research Center, Moffett Field, California 94035-1000

An experiment documenting the compressible flow over a dynamically deforming airfoil is presented. This airfoil, which has a leading-edge radius that can be dynamically changed, was tested at various deformation rates for fixed airfoil angle of attack. Selected leading-edge shapes were also tested during airfoil oscillation. These tests show that for a range of Mach numbers observed on the retreating blades of helicopter rotors the dynamic stall vortex can be avoided by a judicious variation of leading-edge curvature.

Nomenclature

C_p = pressure coefficient
$C_{p_{\min}}$ = peak suction pressure coefficient
c = airfoil chord
f = frequency of oscillation, Hz
k = reduced frequency, $\pi f c/U_\infty$
M = freestream Mach number
s, n = distance along and normal to surface
t = time
U_∞ = freestream velocity
V = velocity of dynamically deforming leading-edge motion
x, y = chordwise and vertical distance
α = angle of attack
ν = kinematic viscosity
ρ = fluid density
Ω = z component of vorticity

I. Introduction

THE strong pitching moment that accompanies dynamic stall is well known to be highly detrimental to helicopter performance. Furthermore, compressibility effects induce a premature onset of dynamic stall at freestream Mach numbers as low as 0.3, which greatly limits the performance of a rotor. Presently, a helicopter is restricted from flying at these conditions; therefore, the dynamic lift that is generated by the rapid pitch-up of a rotor blade remains unharnessed. The phenomenon of unsteady flow separation also limits the operational envelope of fixed-wing aircraft when it is encountered during aeroelastic flutter, buffet, etc. Control of both steady and unsteady flow will expand the flight envelopes of future aircraft designs. Recent studies have shown that compressible dynamic stall can be caused either by an extremely strong adverse pressure gradient in the flow near the leading edge or by a shock-induced separation occurring in this region.[1] Because both phenomena are a consequence of the fixed-airfoil geometry, there appears no simple way to significantly alter these conditions. However, the use of smart materials and actuators offers the possibility of designing wings that can continuously and rapidly adapt to changes in local flow conditions, thereby enabling these wings to deliver optimum performance at each instantaneous flow condition. The research being reported here focuses on the fluid dynamic aspects and consequences of such an approach. The dynamic-stall-control efforts previously reported[2–5] are still unproven for compressible flow conditions, except for the work described in Refs. 5 and 6.

Upon recognizing that dynamic stall at practical Mach numbers is induced by rapid flow acceleration followed by abrupt deceleration around the leading edge, a control strategy was developed to modify the flow gradients by suitably shaping the airfoil leading edge. The goal was to reduce the local Mach number in the leading-edge region and to favorably alter the leading-edge pressure distribution, thereby introducing possible delays or elimination of the onset and effects of dynamic stall. This approach has led to the concept of the dynamically deforming leading-edge (DDLE) airfoil, which has been fully described in Ref. 6. The leading-edge curvature of the DDLE airfoil can be changed dramatically in real time by a small chordwise movement of the airfoil leading edge, which causes pronounced effects on the aerodynamic behavior of the airfoil. A wider flight envelope can be realized with significantly improved performance, if the airfoil can be continuously deformed to adapt to the instantaneous flow conditions. However, many fluid dynamics issues need to be resolved for these instantaneous geometry changes to be implemented. As has been shown by Reynolds and Carr,[7] the vorticity flux through a boundary layer is proportional to the potential flow pressure gradient over the surface. When using an adaptive wing for flow control, the dominant timescale affecting the fluid physics, and in particular the vorticity balance in the flow, is the rate of change of the surface geometry. Because the vorticity flux depends on the surface pressure distribution, however, control of unsteady separation is influenced by the ability of the flow to adjust to the instantaneous surface shape. The feedback between the shape and surface pressure distribution will determine the control strategy. A series of building block experiments is under way to establish the existence of a suitable strategy for unsteady stall control. These experiments are being conducted by the Navy–NASA Joint Institute of Aeronautics in the Compressible Dynamic Stall Facility (CDSF) located at the Fluid Mechanics Laboratory of NASA Ames Research Center. Reported here are the results of the first two such experiments. The first experiment was a parametric investigation of the flow at various angles of attack over a range of leading-edge shapes and shape-change histories. The results of

Presented as Paper 97-2236 at the AIAA 15th Applied Aerodynamics Conference, Atlanta, GA, June 23–25, 1997; received Feb. 3, 1998; revision received July 1, 1998; accepted for publication July 8, 1998.

*Associate Director and Research Professor, Navy–NASA Joint Institute of Aeronautics, Department of Aeronautics and Astronautics; mailing address: M.S. 260-1, NASA Ames Research Center, Moffett Field, CA 94035. Associate Fellow AIAA.

†Senior Research Scientist, Navy–NASA Joint Institute of Aeronautics. Member AIAA.

‡Research Scientist and Group Leader, Unsteady Viscous Flows, Aviation Research, Development and Engineering Center, U.S. Army ATCOM and Fluid Mechanics Laboratory Branch. Member AIAA.

these experiments identified several leading-edge shapes that delivered remarkable steady flow performance. The second experiment reported examined the dynamic-stall characteristics of oscillating airfoils having these fixed shapes and identified certain shapes that do not experience dynamic stall.

II. Description of the Experiment

A. DDLE Airfoil

The DDLE airfoil used was a 6-in. chord airfoil with a NACA 0012 profile when in its initial state (shape 0). The leading-edge curvature could be changed continuously by up to 320%, resulting in a different airfoil profile for each instantaneous leading-edge curvature. The model provides the possibility for real-time adaptation of the airfoil shape in response to changing flow conditions. The leading-edge region of the DDLE airfoil is made from a 0.002-in. carbon fiber composite skin, which progressively thickens over the first 20% of the airfoil. The rest of the airfoil is made from solid aluminum, as shown in Fig. 1. The composite fiber skin is cast with a tang inside the leading edge for attachment to a mandrel contoured to the leading-edge profile of a 6-in. chord NACA 0012 airfoil. The mandrel is part of a thin truss placed inside the airfoil and connected to two ac brushless servomotors through connecting rods entering from each side of the test section. The motors drive the linkage, which translates the truss along the chord line. As noted earlier, a very small movement of the leading edge produces a large change in shape. For example, in a total chordwise movement of only 0.08 in. ($x/c = 0.0133$), the leading-edge profile changes from that of a NACA 0012 airfoil to a semicircular shape, corresponding to a 320% change in leading-edge radius. Programmable motion controllers equipped with digital encoders permit manipulation of the airfoil leading-edge curvature at many rates.

Figure 2 shows some leading-edge shapes attained with the present design that are of relevance to this paper. (Only for the semicircular shape is the inward bump seen, which is attributed to the use of a filler material for bridging the minute gap between the upper and lower surface skins. It is not considered to be a problem because this shape is never used.) Each integer shape change corresponds to a rearward movement of the leading edge by $x/c = 0.0005$ (0.003 in.) from its previous position, with shape 0 being nearly identical to a NACA 0012 airfoil. A shape-change sequence can be completed in less than 50 ms; therefore, shape-change sequences can be phase locked with the airfoil oscillation for oscillation frequencies up to 20 Hz (reduced frequency of $k = 0.1$ for the 6-in. airfoil at $M = 0.3$). Reference 8 provides additional details of the DDLE airfoil design and fabrication.

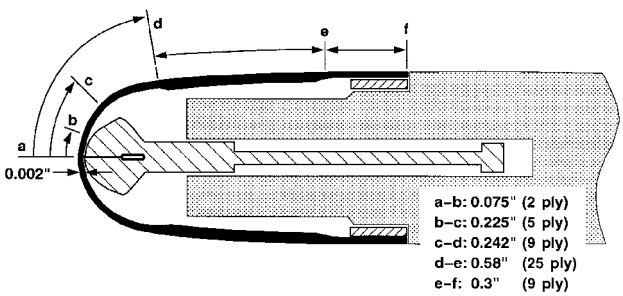

Fig. 1 Construction details of the DDLE airfoil model.

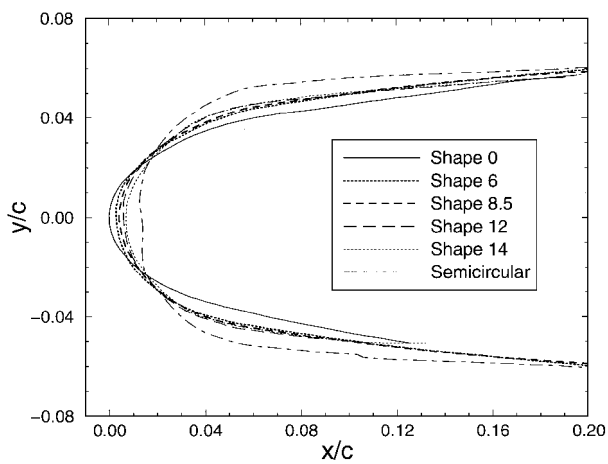

Fig. 2 DDLE airfoil shape profiles.

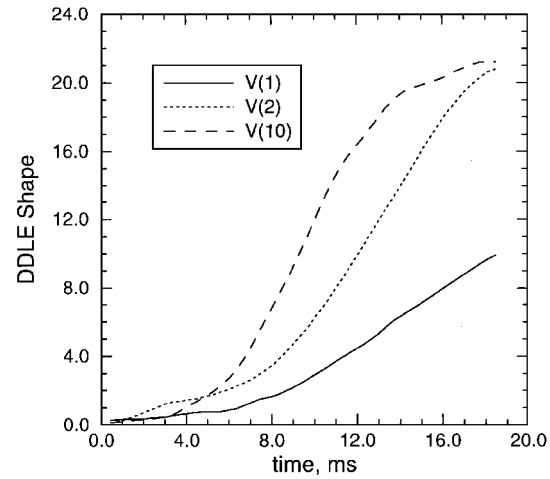

Fig. 3 DDLE shape-change history.

B. Experimental Facility and Technique

The CDSF is an indraft wind tunnel with a 10×14 in. test section. It is equipped with a drive for producing a sinusoidal variation of airfoil angle of attack. In the present study the 6-in. chord, DDLE airfoil was mounted between two metal ports with optical glass inserts to provide visual access to the first 40% of the airfoil chord. The DDLE drive system was mounted on the exterior side walls of the test section. The position histories used in the present experiments are shown in Fig. 3, where $V(m)$ is the rate at which the leading edge is pulled back from its most forward position and m is a rate parameter (the stepper motor revolutions per second) in the control logic used for moving the leading edge. The fastest rate studied, $V(10)$, corresponds to full displacement in 15 ms $[V(10)/U_\infty = 16.5 \times 10^{-6}]$, whereas full displacement takes 40 ms at $V(1)$, $[V(1)/U_\infty = 6.3 \times 10^{-6}]$. Note that $V(0)$ corresponds to the case of no DDLE motion and represents measurements made for fixed-leading-edge shapes.

The experimental data were obtained using the real-time technique of point diffraction interferometry (PDI),[9] which provides instantaneous, quantitative, flowfield density information, from which both surface and global pressure distributions can be derived. The PDI optical arrangement is similar to that of a schlieren system and is described in Ref. 9. The interferograms were analyzed (semiautomatically) by custom image processing software on an IRIS workstation. Because the boundary layer is still thin prior to the onset of dynamic stall, isentropic flow relations were used to convert the densities to pressures.

C. Experimental Conditions

Steady flow interferograms were obtained at $M = 0.3$ and 0.4, when the shapes were fixed at several different radii, at angles of attack of from 8 to 18 deg. Two different unsteady experiments were also conducted. In the first, the effect of changing the leading-edge curvature at different rates on the flow over the airfoil while positioned at a fixed angle of attack of 18 deg was studied to determine whether there were any preferred rates that would offer the most potential for unsteady flow control. PDI images were recorded at $M = 0.3$ for various instantaneous shapes as the airfoil leading edge was retracted at different rates. In the second unsteady flow experiment, PDI images were acquired for fixed shapes 7.5, 8, and 8.5 at $M = 0.3$ and for shapes 6 and 3 at $M = 0.4$ while the airfoil was oscillated at a reduced frequency of $k = 0.05$.

D. Experimental Uncertainties

The estimated uncertainties in the data are as follows:

Mach number ± 0.005

Angle of attack 0.05 deg

Reduced frequency 0.005

$C_p \pm 0.1$ at $M = 0.3$

$C_{p_{\min}} \pm 0.5$ at $M = 0.3$ and ± 0.275 at $M = 0.4$

$\mathrm{d}C_p/\mathrm{d}(x/c) \pm 25$

The uncertainty in C_p depends on the fringe number under consideration and is one fringe for the flow in general, with up to three fringes undetectable near the suction peak at $M = 0.3$. Because the correction for solid and wake blockage was less than 5% for $C_{p_{\min}} = -6.0$ at $M = 0.3$, no corrections were applied to the pressures derived from the PDI images. The gradients were obtained by fitting a spline curve to the pressure distributions and calculating the derivatives of the spline at the locations where the pressure values were recorded. The uncertainty value for the pressure gradient is based on possible differences in the spline fits to the data locally. The airfoil leading-edge displacement was estimated from a calibration procedure performed for the no-flow case.

III. Results and Discussion

A. Characterization of DDLE Flow Regimes, $M = 0.3$

The flow behavior of the DDLE airfoil was mapped as a function of angle of attack and leading-edge shape both for static shapes and for rapid shape changes. In all cases, the airfoil was brought to a fixed angle of attack and held there while the leading-edge shape was varied. Each static shape was held for several seconds before the flow was imaged. For the unsteady cases, the leading edge was rapidly pulled back from shape 0 according to the shape histories plotted in Fig. 3, and the flow was conditionally sampled during the leading-edge motion by phase locking the PDI system to one operator-defined shape per motion.

The results of these parametric studies are presented as flow regime maps in Fig. 4. The interferograms representative of the various flow regimes are shown in Fig. 5. These images are for the $V(1)$ leading-edge motion case, and their respective locations in the shape-number-α parameter space are indicated in Fig. 4b. Figure 4a shows the flow regimes that were observed for the static leading-edge shapes [referred to as $V(0)$, as noted earlier]. Shape 0, corresponding nominally to the NACA 0012 profile, first shows separation at $\alpha = 14$ deg. The separation is from the trailing edge, but significant suction pressure is observed over the leading edge, indicating that the airfoil is producing lift (region T1 in Fig. 4a). As the angle of attack is increased, the separation progresses upstream and the leading-edge suction pressure decreases (region T2), until at 17.5-deg angle of attack, the flow separates from the leading edge with a complete loss of airfoil lift (L). Note that the angle of attack at which any separation is observed increases significantly with decreasing leading-edge sharpness. This trend continues up to shape 8, for which no separation is observed until $\alpha = 17$ deg, although significant leading-edge suction remains until the airfoil reaches 18-deg angle of attack. This region of leading-edge suction at high angle of attack remains for shapes up to shape 12, although a high-frequency vortex-shedding phenomenon appears at these higher-number shapes.

Abrupt leading-edge stall occurs at larger leading-edge displacements; in fact, stall occurs at α as low as 10 deg for shape 10. It is clear from Fig. 4a that stall can be delayed up to an angle of attack of 18 deg for a range of airfoil shapes around shape 8. It can also be seen that separated flow at high α can be made to reattach by simply rounding the leading edge.

Rapidly changing the leading-edge shape at a fixed angle of attack results in the development of a flow pattern very suggestive of the dynamic stall of an oscillating airfoil. This pattern is shown with the interferograms (Fig. 5) accompanying the flow regime map for leading-edge displacement at the rate $V(1)$ (Fig. 4b). These images

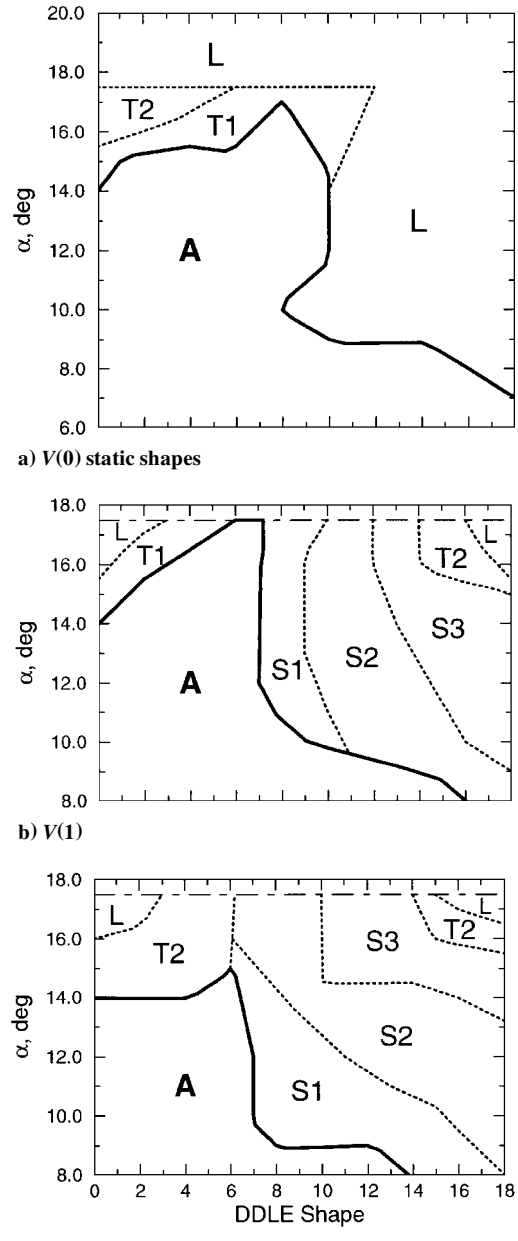

Fig. 4 Flow regimes over the DDLE airfoil; $M = 0.3$ and $k = 0$.

show the flowfield up to $x/c \approx 0.25$. The flow behavior at $V(1)$ is not significantly different from that observed for fixed shapes (Fig. 4a) for shapes up to shape 6. Beyond shape 6 a fringe pattern similar to incipient dynamic stall vortex formation appears (denoted as S1 in Fig. 4b; Fig. 5b). This becomes an organized structure that grows in size (regime S2; Fig. 5c) and moves downstream along the airfoil surface (regime S3; Fig. 5d). Only at angles of attack greater than 15 deg and for shapes rounder than shape 16 was complete leading-edge stall observed (Fig. 5f).

The flow regimes observed while changing the leading-edge shape at the highest rate studied [$V(10)$] are shown in Fig. 4c. Again, as for rate $V(1)$, a dynamic-stall-like vortex develops for shapes above shape 6; however, the fully attached flow regime is limited to angles below 14 deg, the static stall angle observed for the NACA 0012 profile. This shrinkage of the attached flow regime suggests that a lower deformation rate is preferable at this freestream condition.

B. Development of Peak Suction Pressure, $M = 0.3$

Figures 6a and 6b show the development of leading-edge peak suction pressure at $\alpha = 7.98$ and 17.5 deg for different leading-edge deformation rates in steady flow at $M = 0.3$. Because the flow is attached at $\alpha = 7.98$ deg (Fig. 6a), the variation in deformation rate

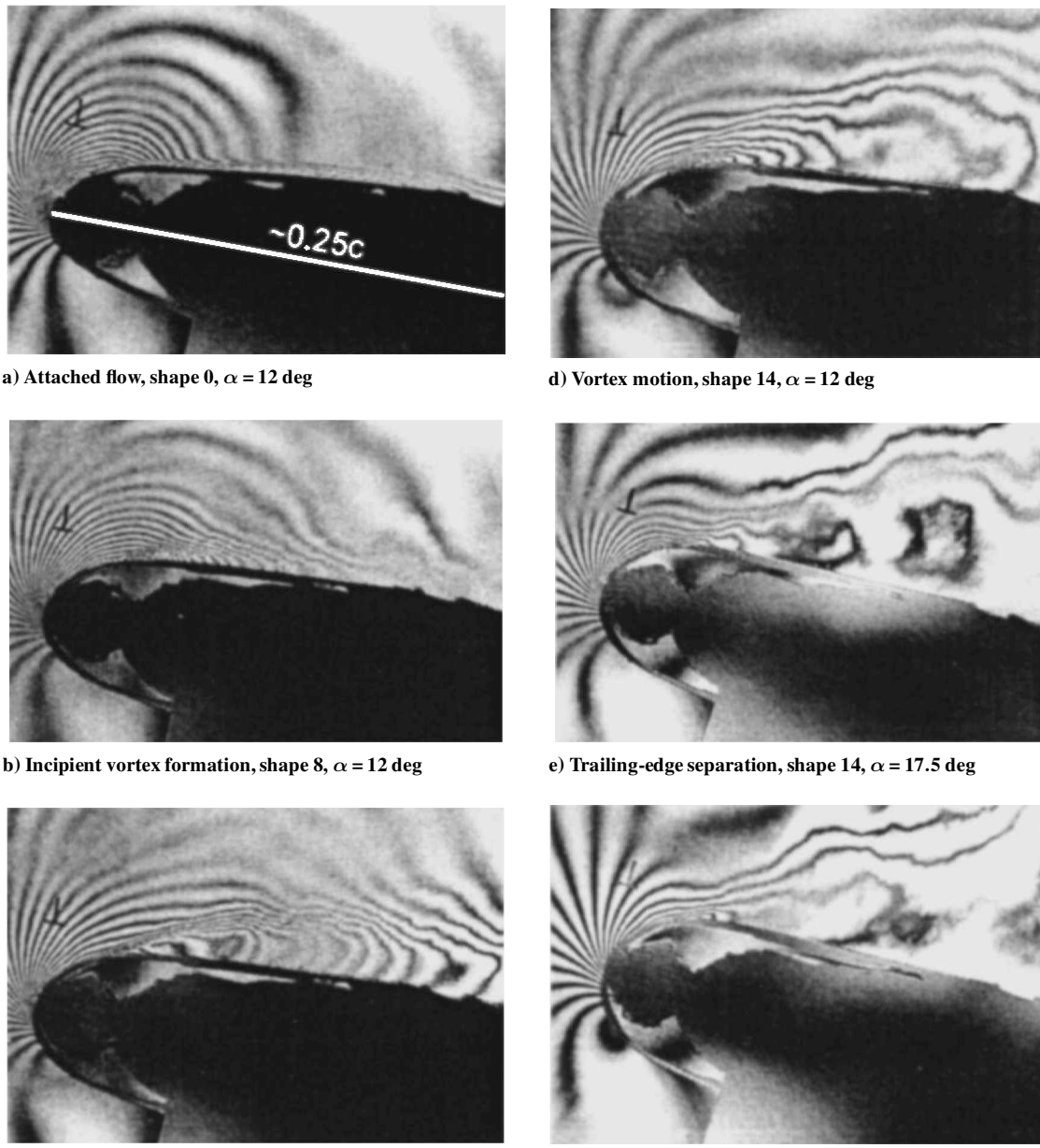

a) Attached flow, shape 0, α = 12 deg

d) Vortex motion, shape 14, α = 12 deg

b) Incipient vortex formation, shape 8, α = 12 deg

e) Trailing-edge separation, shape 14, α = 17.5 deg

c) Vortex growth, shape 10, α = 12 deg

f) Leading-edge separation, shape 18, α = 17.5 deg

Fig. 5 PDI images illustrating the various flow regimes of Fig. 4b; M = 0.3, k = 0, and V(1).

does not have a major effect. Only a slight delay of peak suction development is seen for $V(1)$, $V(2)$, and $V(10)$. The flow at $V(0)$ is in an equilibrium state and, thus, develops a higher level of suction. In contrast, at a high angle of attack, when the flow is initially separated, dramatic differences are seen for the different rates used (Fig. 6b). Results for rate $V(1)$ are similar to those for rate $V(0)$, where the surface curvature is fixed at each shape. The flow reattaches and can develop very high suction levels for shapes 5–7 when tested statically [$V(0)$] and for shapes 5–11 for rate $V(1)$. On the other hand, the peak suction level increases steadily for most shapes at rates $V(2)$ and $V(10)$, but it never reaches the high values seen for $V(0)$. The low values of $C_{p_{\min}}$ and the similarity for rates $V(2)$ and $V(10)$ suggest that rate $V(1)$ is essentially a quasisteady equivalent to $V(0)$ and is to be preferred for reattaching the flow if it separates. Very rapid deformation rates are not beneficial in such a case.

C. Flow Details over DDLE Shape 8.5 Airfoil, M = 0.3, k = 0.05

As discussed for Fig. 4a, there exists a range of airfoil shapes in flow at $M = 0.3$ in which flow separation is delayed up to $\alpha = 18$ deg for the steady conditions. Thus, it appears useful to investigate the behavior of an oscillating airfoil with a fixed-nose shape within this range as the next step in assessing the effectiveness of the DDLE airfoil concept for achieving dynamic stall control. Several airfoils having leading-edge shapes similar to shape 8 were tested while executing sinusoidal pitching oscillations. In the tests, the DDLE leading-edge curvature was held fixed at a predetermined value. Flow images over the shape 8.5 airfoil will be presented later because this shape provided the maximum delay of unsteady separation; note that the flows over shapes 7.5 and 8 were qualitatively similar.

The PDI image in Fig. 7a for $\alpha = 10.98$ deg indicates that the flow is attached everywhere because the fringes turn smoothly around the airfoil nose and return gradually toward the surface. The boundary-layer fringes run nearly parallel to the surface, a pattern observed in prior tests during attached flow conditions. Because the fringes represent constant density lines and the flow is attached, the image also presents global and surface pressure information. A similar flow pattern is present even at $\alpha = 17.02$ deg (Fig. 7b). (Note that there is some separation downstream of the leading edge, but the flow near the leading edge is attached.) For comparison, deep dynamic stall was found to occur[9] by $\alpha = 16$ deg over an oscillating NACA 0012 airfoil at these same flow conditions, with a corresponding loss in leading-edge suction, whereas in the present case, the flow near the leading edge is still attached at 17 deg. At $\alpha = 19.02$ deg (Fig. 7c), a larger region of separated flow can be seen toward the rear of the

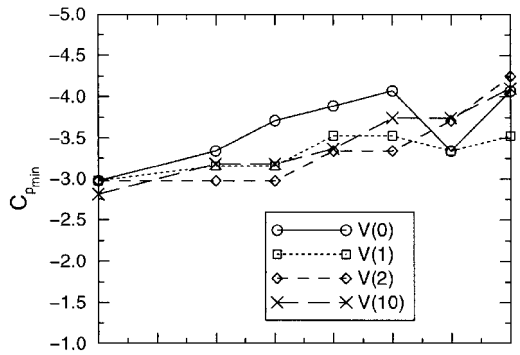

a) $\alpha = 8$ deg

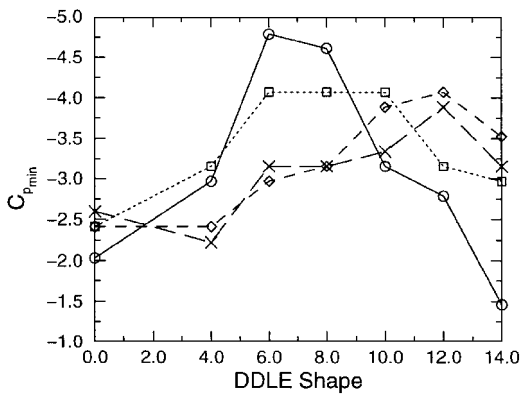

b) $\alpha = 17.5$ deg

Fig. 6 Effect of deformation rate on airfoil peak suction; $M = 0.3$ and $k = 0$.

airfoil, but even at this high angle of attack, the leading-edge flow is fully attached. The separation seen in the image is trailing-edge flow reversal moving upstream. Figure 7d shows that the leading-edge flow is attached also at $\alpha = 20.0$ deg; this is a major improvement of the flow behavior. An even more important result is the absence of the dynamic stall vortex in the separated flow region in complete contrast to what is normally seen on oscillating airfoils. Thus, for the DDLE shape 8.5 airfoil it has been possible to maintain a vortex-free flow at all angles of attack during oscillation. This is a significant result because the strong and detrimental pitching moment variations concomitant with a convecting vortex have now been eliminated on this single-element airfoil, even at high angles of attack. The attached leading-edge flow allows the airfoil to continuously produce suction lift throughout the upstroke. During the downstroke, the flow reattaches toward the trailing edge [Figs. 7e ($\alpha = 15.49$ deg) and 7f ($\alpha = 13.97$ deg)]. Because the airfoil develops less lift at the lower angles of attack, the leading-edge vorticity must be shed, which seems to happen through the occurrence of light dynamic stall over a small angle-of-attack range, based on analysis of the interferograms. In Fig. 7f, the fringe pattern seen near the leading edge confirms this, as the airfoil flow adapts to this lower angle of attack.

In summary, although the airfoil experienced stall, it is a much softer stall wherein the flow over the leading edge remains attached and the vorticity developed at high angles of attack is shed through mild trailing-edge stall.

D. Development of Airfoil Peak Suction for Selected DDLE Shapes, $M = 0.3, k = 0.05$

The peak suction pressures during airfoil oscillation have been plotted as a function of angle of attack in Fig. 8 for the NACA 0012 and DDLE shape 7.5, 8, and 8.5 airfoils. The peak suction develops at a much lower rate for the DDLE shapes shown than for the NACA 0012 airfoil and, hence, stall onset is delayed to higher angles of attack. The shape 8.5 airfoil experiences a gradual loss of peak suction, which points to a softer stall development. The flow remains in the light stall state, over a larger angle-of-attack range for shapes 7.5 and 8. The fluctuations in the peak suction values in the poststall state can be attributed to the intermittent reattachment of the leading-edge flow for these cases.

E. Airfoil Pressure and Vorticity Flux Distributions, $M = 0.3, k = 0.05$

Figures 9a and 9b present the static pressure distributions over the airfoil for the upstroke from $\alpha = 11$ to 20 deg and for the downstroke from $\alpha = 20$ to 10 deg. The distribution at 11.02 deg shows a suction peak C_p of about -4.0, which is considerably less than the value of about -6 that was observed for the NACA 0012 airfoil, as shown in Fig. 8. But a more interesting feature is the occurrence of the peak at $x/c \approx 0.05$, whereas for the NACA 0012 airfoil it was very close to the leading edge.[1] As the angle of attack is increased to 15 deg, the suction peak moves closer to the leading edge. However, as the pressure recovers from this value, a plateau develops from $x/c \approx 0.06$. The plateau shrinks as the angle of attack is increased to 17 deg; this behavior is consistent with the formation of a separation bubble. This feature was also observed on the NACA 0012 airfoil, where bursting of the bubble resulted in dynamic stall onset. Further increase in angle of attack reduced the peak suction pressure, which can be attributed to the upstream movement of the trailing-edge separation and a gradual spread of the separated region over the airfoil. A C_p value of about -4.5 is seen at $\alpha = 20$ deg. On the downstroke (Fig. 9b), the pressure minimum continues to decrease, but by about 19 deg, a second peak develops in the distributions and the plot for $\alpha = 15.5$ deg shows the plateau spreading toward the trailing edge. At lower angles of attack, the vorticity is shed through light dynamic stall, as already discussed, and by 10 deg, the flow once again reaches a state similar to what was seen on the upstroke for 11-deg angle of attack. However, as Fig. 8 shows, the airfoil has to pitch-down to about 8 deg before the suction peak attains the same value measured during the upstroke. These developments are considerably different from those seen for the NACA 0012 airfoil, and as a consequence, the vorticity distributions over the airfoils will also be different.

As described by Reynolds and Carr,[7] when no transpiration is present, the vorticity flux in a flow with a moving surface is given in simplified form by

$$\nu \frac{\partial \Omega}{\partial n} = \frac{\partial U_s}{\partial t} + \frac{1}{\rho}\frac{\partial p}{\partial s}$$

An order of magnitude analysis shows that the surface acceleration term in the equation is about two orders of magnitude smaller and, hence, can be neglected initially. Thus, one can obtain the vorticity fluxes from the pressure distributions by simply taking the derivative with respect to distance along the airfoil surface.

The vorticity fluxes calculated from the pressure distributions are plotted in Figs. 10a and 10b for the DDLE shape 8.5 airfoil and Fig. 10c for the NACA 0012 airfoil. The distributions in Fig. 10a for the airfoil upstroke show that generally there are two peaks in vorticity flux for the higher angles shown: a larger-amplitude, narrow one at the suction peak location and a smaller-amplitude, wider one farther downstream. For smaller angles, the two peaks are away from the leading-edge region. The larger peaks shown have about twice the amplitude of the smaller peaks, but the latter are several times wider. Because the area under the curve gives the total vorticity production, the broader distributions provide a greater contribution to this term. As the angle of attack increases, the second peak moves progressively closer to the leading edge; for example, it is at $x/c = 0.08$ for $\alpha = 11.02$ deg and at $x/c = 0.04$ for $\alpha = 19$ deg. As the airfoil reaches the top of the cycle, there is a reduction in the peak vorticity flux that is produced because the degree of unsteadiness decreases to zero. Also, the data indicate a movement of the vorticity flux peaks toward the trailing edge for $\alpha = 19.59$ and 20 deg. The maximum value indicated in the graph is about 230 for the first peak for $\alpha = 17$ deg, but generally the value for most distributions in the second peak is around 100–125. The decrease in the first peak for $\alpha \geq 17$ deg may be attributable to the trailing-edge separation that was discussed in Sec. III.C.

During the airfoil downstroke, the peak values drop as the angle of attack is decreased, and the peak also moves toward the trailing edge. Note that the vorticity has to decrease due to the decreasing

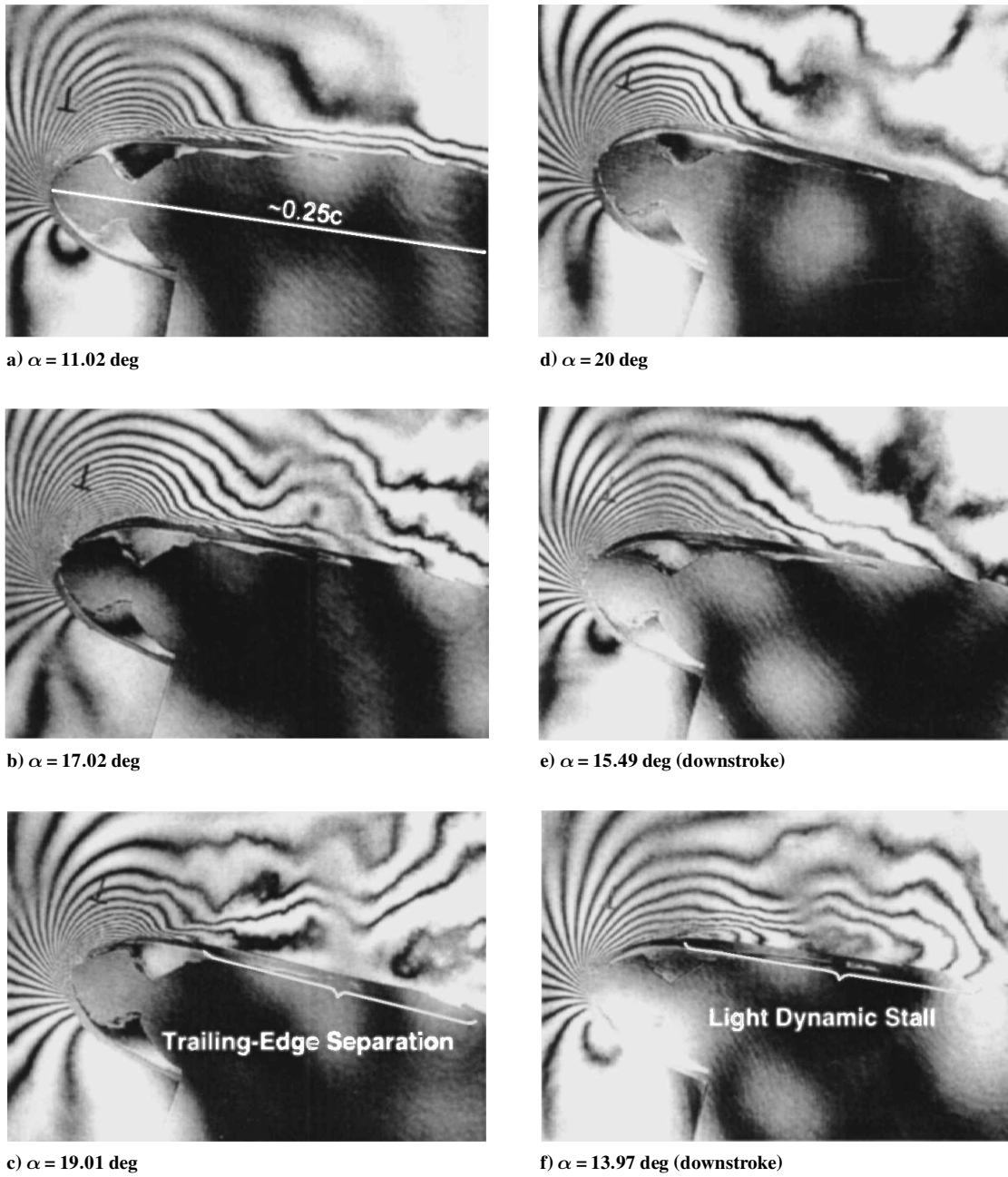

a) α = 11.02 deg

d) α = 20 deg

b) α = 17.02 deg

e) α = 15.49 deg (downstroke)

c) α = 19.01 deg

f) α = 13.97 deg (downstroke)

Fig. 7 PDI images of the DDLE shape 8.5 airfoil; M = 0.3 and k = 0.05.

angle of attack, and the excess vorticity has to be shed for the flow to adjust to the rapidly changing conditions. In Fig. 10c the distribution of vorticity flux for the NACA 0012 airfoil peaks with a magnitude of around 250. At a low angle of attack of 8 deg, this peak is centered around $x/c = 0.04$, but it moves close to the leading edge and is around $x/c = 0.025$ for 13 deg with a magnitude of about 350. The PDI images (not shown here) of Ref. 1 show that dynamic stall ensued at $\alpha = 14$ deg for this case. Also, no trailing-edge separation could be identified in the PDI images of the NACA 0012 for this case; the trailing-edge separation appears to provide a mechanism for shedding the vorticity at the high angles at which the DDLE airfoil was tested. It is believed that, for the vorticity to coalesce into a vortex, these sharp high peak values are necessary. The vortex thus formed has to be convected by the flow. Eventually, flow separation follows, causing unacceptably large hysteresis in the load and moment loops. By carefully lowering the peak levels and distributing the total vorticity over a greater area on the airfoil upper surface, it becomes possible to keep the flow attached and produce lift at low drag values until higher angles of attack, as was demonstrated in the case of the DDLE airfoil.

F. Characteristics of the DDLE Airfoil Flow at M = 0.4, Steady Flow

Figure 11 shows the flow regimes as a function of static airfoil leading-edge curvature and static angles of attack in steady flow at $M = 0.4$. Based on comparisons of interferograms (not shown) the flow over the shape 0 airfoil is similar to that over the NACA 0012 airfoil. Shocks develop in this flow at around 10-deg angle of attack, and the airfoil experiences leading-edge stall at around 14 deg (L in Fig. 11). As the nose radius is increased at $\alpha = 6$ deg, the flow remains attached until shape 12 is reached. For angles of up to 13 deg and shapes up to 4, shocks are present in the flow, but the flow does not separate; this regime is A_S in Fig. 11. A fringe counting shows that the Mach number is as high as 1.2 at the foot of the shocks. Eventually, the shocks induce a small-scale separation above 12 deg for shapes 4 and beyond ($S1_S$). Even with the shocks present over the upper surface, the flow remains in that state until angles of attack of about 17 deg, when leading-edge stall occurs. This stall angle is much higher than the 14-deg stall angle observed for the NACA 0012, showing the considerable alleviation of separation that can be obtained by rounding the leading edge. The small-scale separation grows progressively more severe for rounder leading-edge shapes

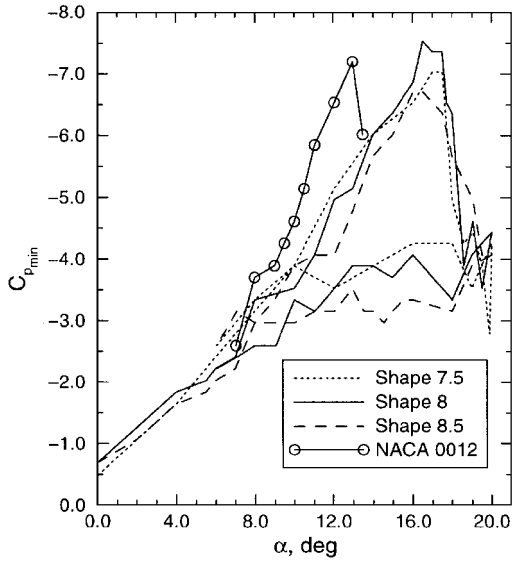

Fig. 8 Development of peak suction pressure for different DDLE airfoil shapes; $M = 0.3$ and $k = 0.05$.

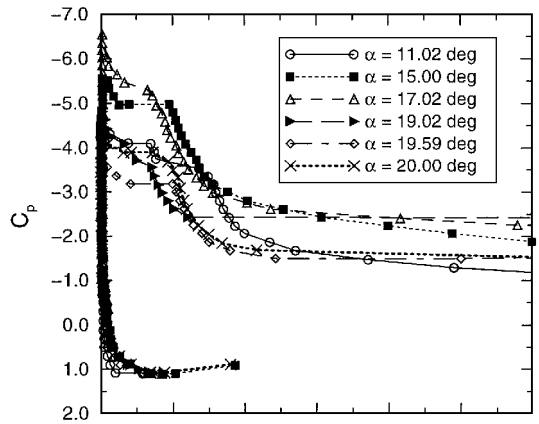

a) Upstroke

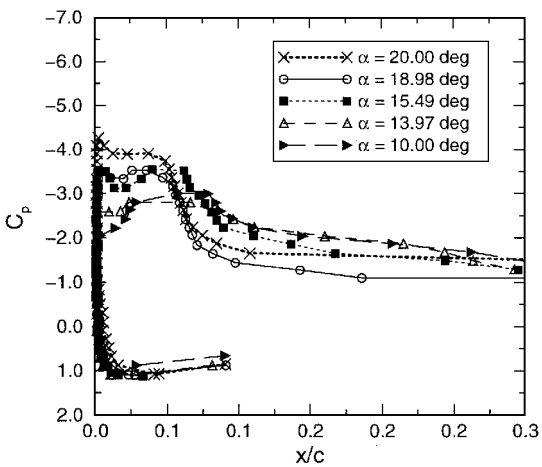

b) Downstroke

Fig. 9 Pressure distributions on the oscillating DDLE shape 8.5 airfoil; $M = 0.3$ and $k = 0.05$.

(regimes $S2_S$ and $S3_S$), and eventually complete separation from the leading edge is observed.

G. PDI Images of DDLE Airfoil Shape 6 Flow, $M = 0.4$, $k = 0.05$

Although the shape 8.5 airfoil displayed excellent flow characteristics at $M = 0.3$ and $k = 0.05$, dynamic stall with a well-formed dynamic stall vortex occurred on this shape at $M = 0.4$ and $k = 0.05$ (not shown). Because shape 8.5 was on the border of the envelope of attached flow with shocks in steady flow (Fig. 11), sharper leading-edge shapes were studied. Results showed that the DDLE shape 6 airfoil behaved at $M = 0.4$ in a manner similar to the shape 8.5 airfoil at $M = 0.3$ and $k = 0.05$. Representative interferograms for this flow are presented in Figs. 12a–12f. At an angle of attack of 8 deg, Fig. 12a shows that the flow is fully attached, with a $C_{p_{min}}$ of -2.92. The interferograms showed a fringe pattern with two peaks by $\alpha = 10$ deg (not shown). The critical C_p of -3.66 was also exceeded by this angle, and shocks appeared at higher angles. Figure 12b shows the multiple shocks, which formed at $\alpha = 11.98$ deg. Some flow disturbances can be seen at the foot of the last shock in Fig. 12b; however, the fringes indicate attached flow. This flow pattern continued until $\alpha = 16$ deg, when trailing-edge separation was seen (not shown). Figure 12c shows for $\alpha = 18$ deg that the leading-edge flow is still attached, although with fewer fringes, and shows

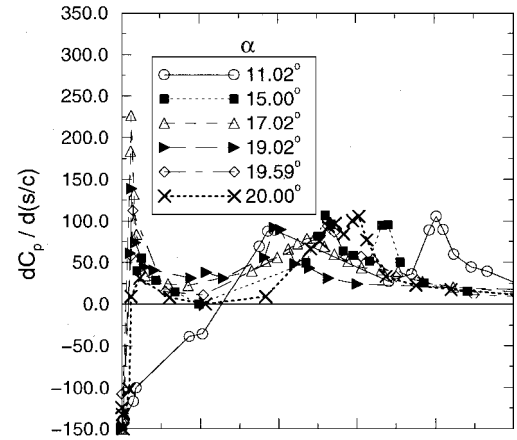

a) DDLE shape 8.5 airfoil, upstroke

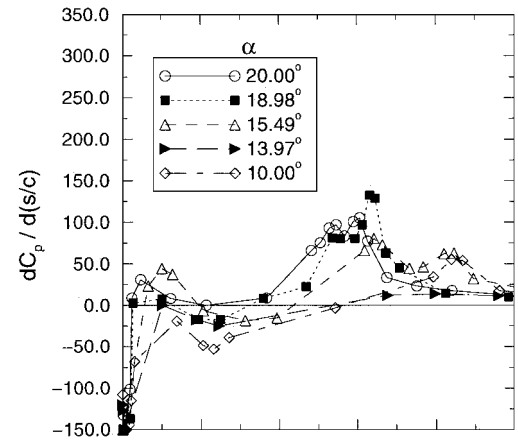

b) DDLE shape 8.5 airfoil, downstroke

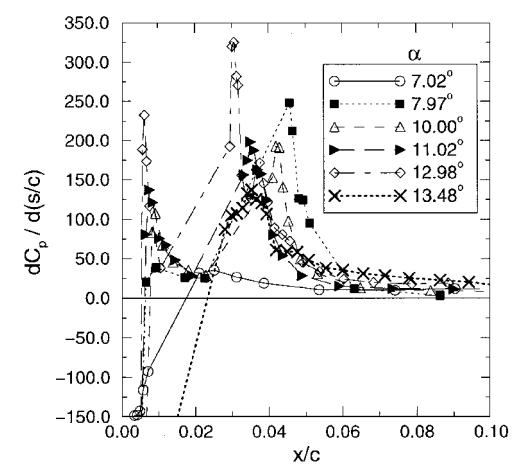

c) NACA 0012 airfoil

Fig. 10 Vorticity flux distributions; $M = 0.3$ and $k = 0.05$.

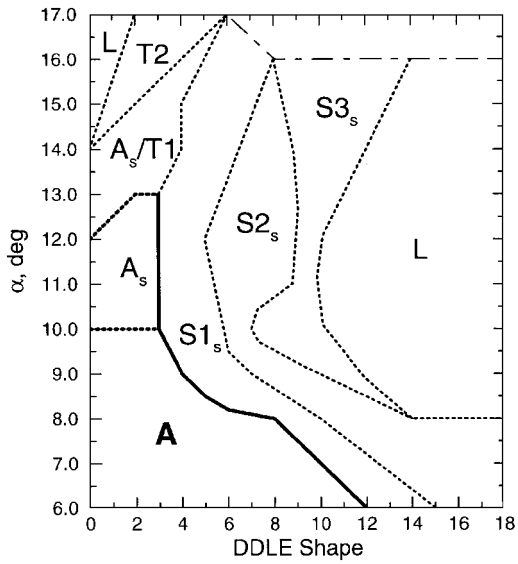

Fig. 11 Flow regimes over the DDLE airfoil; $M = 0.4$, $k = 0$, and $V(0)$.

some trailing-edge separation near $x/c \approx 0.2$. The decrease in the number fringes represents a corresponding decrease in the local peak suction value, which is about -3.24 for this case. It is believed that the increased wake width due to trailing-edge separation has altered the airfoil pressure distribution and has caused the leading-edge flow to become subsonic again. Figure 12d for $\alpha = 20$ deg shows that the trailing-edge separation has progressed to $x/c \approx 0.1$, yet the leading-edge flow remains attached at the top of the upstroke. During the downstroke, the separated portion of the flow reattaches progressively toward the trailing edge. Attached flow can be seen up to $x/c \approx 0.15$ in Fig. 12e for $\alpha = 18$ deg. At an angle of attack of 13.97 deg (Fig. 12f), the flow appears to have fully reattached. However, the tiny, vertical fringes near $x/c \approx 0.08$–0.12 show an incipient vortex, which will eventually evolve to look like the light dynamic stall flow seen for the shape 8.5 airfoil at $M = 0.3$ and $k = 0.05$ (Fig. 6f). It seems that shape 6 provides the conditions to prevent the formation of a deep dynamic stall vortex and the corresponding strong pitching moment variations. The formation of shocks in the flow implies that the stall onset mechanisms for these conditions are significantly different from those at $M = 0.3$. That the DDLE airfoil did not experience dynamic stall even at this Mach number confirms the applicability of the concept for a variety of flow conditions.

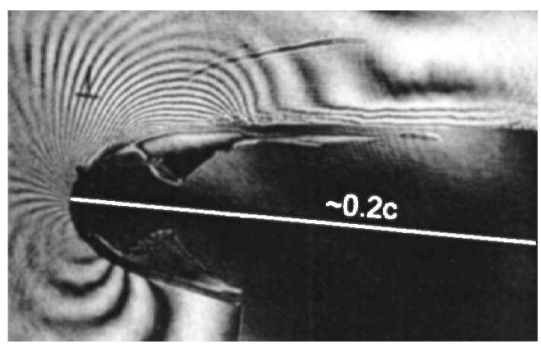

a) $\alpha = 7.97$ deg

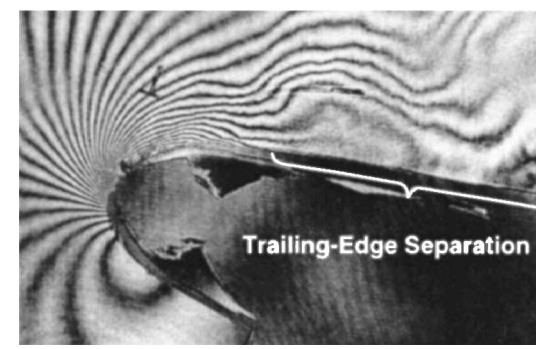

d) $\alpha = 20$ deg

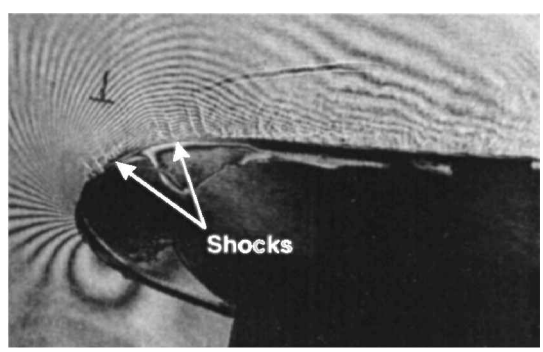

b) $\alpha = 12.03$ deg

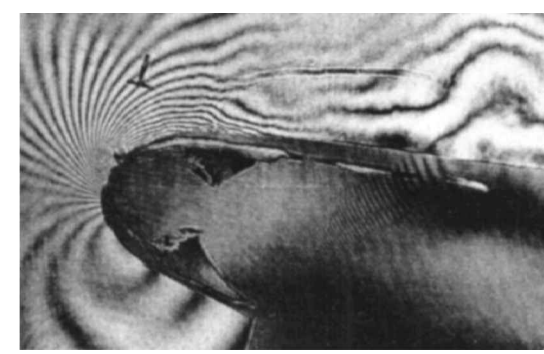

e) $\alpha = 18$ deg downstroke

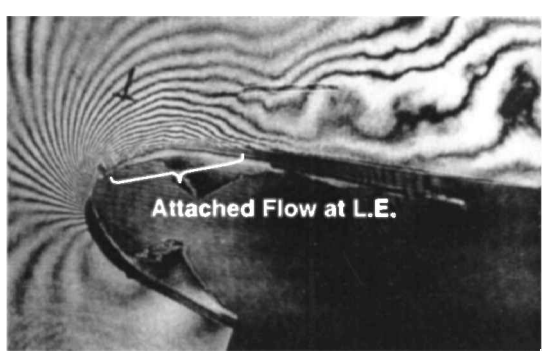

c) $\alpha = 18$ deg

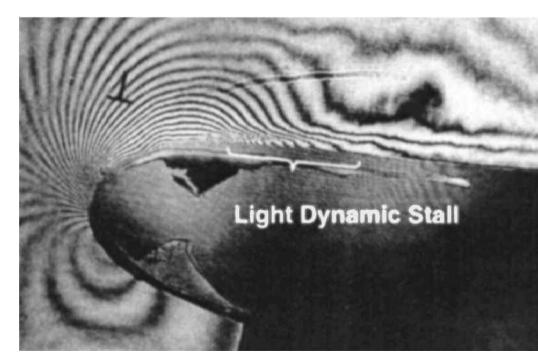

f) $\alpha = 13.97$ deg downstroke

Fig. 12 PDI images of the DDLE shape 6 airfoil; $M = 0.4$ and $k = 0.05$.

IV. Conclusions

The aim of these studies was to achieve control of flow separation and to eliminate dynamic stall vortex through dynamic airfoil leading-edge curvature change and, thus, effect vorticity management in the flow. Hence, a two-part investigation of the unsteady effects of dynamically deforming the leading edge of an airfoil was conducted. In the first part, the effects of dynamic shape change were examined for an airfoil at a fixed angle of attack. The second part focused on the dynamic stall behavior of selected NACA 0012 derivative airfoil shapes. Dynamically changing the airfoil leading-edge curvature showed that it is preferable to change the curvature slowly for the flow to adjust to the instantaneous geometry if control is to be effective. In the case of dynamic stall flow over certain shapes, it was successfully demonstrated that, by carefully selecting a fixed shape for the leading-edge geometry, the dynamic stall vortex was completely eliminated. DDLE airfoils with shape 8.5 at $M = 0.3$ and shape 6 at $M = 0.4$ both were dynamic stall free, and the leading-edge flow was always attached, even though there was some trailing-edge separation present in the flow. This remarkable result, thus, validated the use of the DDLE airfoil concept for achieving dynamic stall control. Future studies will address issues arising from continuous shape change while pitching the airfoil.

Acknowledgments

The project was supported by ARO-MIPR-96-7 to the Naval Postgraduate School and was monitored by T. L. Doligalski, with initial funding from the Air Force Office of Scientific Research. Additional support was received from S. S. Davis, Fluid Mechanics Laboratory, NASA Ames Research Center. The design and fabrication support of C. D. Sticht, C. Hiel, and G. N. Paulson; the dynamically deforming leading-edge (DDLE) control system design of D. D. Squires; and the help of R. A. Miller in model installation are all greatly appreciated.

References

[1] Chandrasekhara, M. S., Wilder, M. C., and Carr, L. W., "On the Competing Mechanisms of Compressible Dynamic Stall," *AIAA Journal*, Vol. 36, No. 3, 1998, pp. 387–393.

[2] Carr, L. W., and McAlister, K. W., "The Effect of Leading-Edge Slat on the Dynamic Stall of an Oscillating Airfoil," AIAA Paper 83-2533, Oct. 1983.

[3] Carr, L. W., McAlister, K. W., and McCroskey, W. J., "Analysis of the Development of Dynamic Stall on Oscillating Airfoil Experiments," NASA TN-D-83820, Jan. 1977.

[4] Allrefai, M., and Acharya, M., "Controlled Leading-Edge Suction for the Management of Unsteady Separation over Pitching Airfoils," AIAA Paper 95-2188, June 1995.

[5] Geissler, W., and Sobieczsky, H., "Unsteady Flow Control on Rotor Airfoils," AIAA Paper 95-1890, June 1995.

[6] Chandrasekhara, M. S., Wilder, M. C., and Carr, L. W., "Control of Flow Separation Using Adaptive Airfoils," AIAA Paper 97-0655, Jan. 1997.

[7] Reynolds, W. C., and Carr, L. W., "Review of Unsteady, Driven, Separated Flows," AIAA Paper 85-0527, March 1985.

[8] Chandrasekhara, M. S., Carr, L. W., Wilder, M. C., Paulson, G. N., and Sticht, C. D., "Design and Development of a Dynamically Deforming Leading Edge Airfoil for Unsteady Flow Control," *ICIASF'97 Record*, IEEE Pub. 97CH36121, Inst. of Electrical and Electronics Engineers, Piscataway, NJ, 1997, pp. 132–140.

[9] Carr, L. W., Chandrasekhara, M. S., and Brock, N., "A Quantitative Study of Unsteady Compressible Flow on an Oscillating Airfoil," *Journal of Aircraft*, Vol. 31, No. 4, 1994, pp. 892–898.

M. Samimy
Associate Editor